Chemosphere 306 (2022) 135611

Contents lists available at ScienceDirect

Chemosphere

journal homepage: www.elsevier.com/locate/chemosphere

Degradation of geosmin and 2-methylisoborneol in UV-based AOPs for photoreactors with reflective inner surfaces: Kinetics and transformation products

Tan Meng [a], Xiao Su [a,b,c,*], Peizhe Sun [a,**]

[a] School of Environmental Science and Engineering, Tianjin University, Tianjin, 300072, China
[b] Tianjin Waterworks Group Co. Ltd., Tianjin, 300040, China
[c] Tianjin Water Group Co. Ltd., Tianjin, 300042, China

HIGHLIGHTS

- Various UV-based AOPs were compared in photoreactor with a reflective inner surface.
- Kinetic model to simulate the degradation of GSM and 2-MIB was established.
- Transformation products of GSM in UV-based AOPs were detected.
- Possible degradation pathways of GSM in UV-based AOPs were proposed.
- Degradation of GSM and 2-MIB were compared in PBS and environmental water sample.

GRAPHICAL ABSTRACT

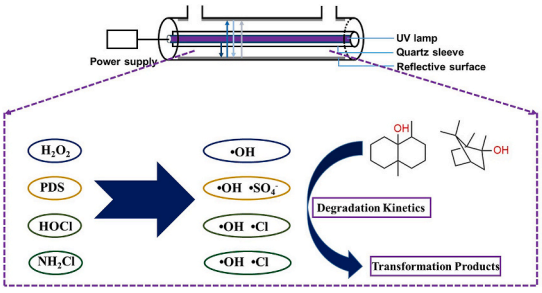

ARTICLE INFO

Handling Editor: Jun Huang

Keywords:
UV-Based advanced oxidation processes
Dynamic model
Geosmin
Engineering photoreactor
Transformation products

ABSTRACT

Geosmin (GSM) and 2-methylisoborneol (2-MIB) are representative musty/earthy odor compounds commonly present in surface water. In present study, the degradation of GSM and 2-MIB subject to different UV-based advanced oxidation processes (AOPs), including UV/H_2O_2, UV/$S_2O_8^{2-}$, UV/chlorine, and UV/chloramine, in a phosphate-buffered saline (PBS) was conducted in a photoreactor with reflective inner surfaces and compared with that in an environmental water sample. A dynamic model to predict the degradation of GSM and 2-MIB in the photoreactor with reflective inner surfaces in the four UV-based AOPs was developed applying the second-order rate constants for the GSM and 2-MIB with *primary reactive species* (i.e., •OH, •Cl, and •SO_4^-) determined in this study. The model was proven to successfully simulate the degradation of GSM and 2-MIB. In addition, 8, 7, 8, and 11 degradation intermediates were detected from UV/H_2O_2, UV/$S_2O_8^{2-}$, UV/chlorine, and UV/chloramine in this study, and possible degradation pathways were proposed. This study is the first to report the degradation kinetics and formation products of GSM and 2-MIB in UV/chloramine. Research based on photoreactors with reflective inner surfaces may provide some guidance for eliminating GSM and 2-MIB in UV-based AOPs for full-scale engineering applications.

Abbreviations: UV-AOPs, UV-Based advanced oxidation processes; GSM, Geosmin.

* Corresponding author. School of Environmental Science and Engineering, Tianjin University, Tianjin, 300072, China.
** Corresponding author.
E-mail addresses: 13821348810@126.com (X. Su), sunpeizhe@tju.edu.cn (P. Sun).

https://doi.org/10.1016/j.chemosphere.2022.135611
Received 25 March 2022; Received in revised form 30 May 2022; Accepted 3 July 2022
Available online 7 July 2022

1. Introduction

Unpleasant odors posed a major threat to traditional drinking water treatment plants worldwide (Omur-Ozbek and Dietrich, 2008; Wang et al., 2019). Geosmin (GSM) and 2-methylisoborneol (2-MIB) are representative musty/earthy odor compounds that mainly generated from *cyanobacteria* or blue-green algae. Typical reported GSM and 2-MIB levels in surface water vary between 5 and 900 ng L^{-1} (Kim et al., 2016). Traditional water treatment technologies such as coagulation, sedimentation, and filtration and common oxidation processes (including Cl_2, ClO_2, and $KMnO_4$) are not effective for removing of GSM and 2-MIB because of their extremely low odor threshold concentrations (4–20 ng L^{-1}) (Agus et al., 2011; Srinivasan and Sorial, 2011). More effective processes are required for eliminating GSM and 2-MIB in drinking water treatment processes.

Ultraviolet (UV)-based advanced oxidation processes (AOPs) have been successfully employed as the effective technologies for eliminating contaminants based on the generation of highly reactive *primary reactive species* (PRS). These UV-based AOPs include processes based on hydroxyl radicals (•OH, 1.8–2.7 V) (UV/H_2O_2), but also those based on other oxidizing species featuring sulfate ($•SO_4^-$, 2.5–3.1 V) (UV/PDS) or chlorine radicals (•Cl, 2.0 V) (UV/HOCl, UV/NH_2Cl) (Eqs. (1)–(5)) (Miklos et al., 2018; Wang et al., 2020). The second-order rate constants for GSM and 2-MIB with •OH and $•SO_4^-$ are 10^9–10^{10} and 10^8 $M^{-1}·s^{-1}$, respectively. Compared with •OH, •Cl is more selective and shows higher reactivity in some instances (Fang et al., 2014). Considering the high reactivity of these PRSs, the application of UV-based AOPs may be a practical and effective technology for the elimination of GSM and 2-MIB. Examples of UV-based AOPs, including UV/H_2O_2, UV/HOCl and UV/PDS, have been shown to effectively degrade GSM and 2-MIB (Jo et al., 2011; Kim et al., 2016; Ma et al., 2018; Wang et al., 2015; Xie et al., 2015). However, few studies have compared the efficiencies of various UV-based AOPs, which is important for selecting suitable treatment process for water treatment plants. Moreover, the newly proposed UV/NH_2Cl, which produces radical species at higher rate due to fast photolysis of NH_2Cl, has never been evaluated for odor compounds removal.

$$NH_2Cl + h\nu \rightarrow •NH_2 + •Cl \quad (1)$$

$$HOCl/OCl^- + h\nu \rightarrow •OH + •Cl \quad (2)$$

$$•Cl + OH^-/H_2O \rightarrow ClOH•^- \rightarrow Cl^- + •OH \quad (3)$$

$$S_2O_8^{2-} + h\nu \rightarrow 2\ •SO_4^- \quad (4)$$

$$•SO_4^- + OH^-/H_2O \rightarrow SO_4^{2-}/\ HSO_4^- + •OH \quad (5)$$

Previous studies have established comprehensive dynamic models for UV-based AOPs, which have been successfully used for the prediction of contaminant degradation in lab-scale reactors with thin optical path lengths. Examples include collimated beam reactors and merry-go-around photoreactors (Fang et al., 2014; Sun et al., 2019; Xie et al., 2015). However, in engineering applications, the photoreactors are designed to absorb as much UV light as possible by applying reflective inner surfaces. With the light reflects between the inner surfaces, the light path length in the engineering photoreactors is considerably increased, which is contrary to the quartz reactor in the laboratory. The lab-scale dynamic model established with a fixed short optical path-length may not be suitable for engineered photoreactors. Therefore, the degradation kinetic should be conducted based on a full-scale system design with relevant operational parameters (i.e., reflective inner surfaces) determined in standardized lab- or pilot-scale experiments.

In addition, although UV-based AOPs are powerful oxidation technologies, the target compounds generally cannot be completely mineralized during the degradation, and several byproducts may be generated. Compared to the extensive research regarding the degradation of GSM and 2-MIB, only a few research have been conducted to investigate the degradation pathways of GSM and 2-MIB under UV-based AOPs. Previous studies reported the degradation of GSM and 2-MIB in UV/HOCl. Among these studies six (Kim et al., 2016) and fourteen (Ma et al., 2018) degradation intermediates have been found, respectively. Transformation pathways of UV/H_2O_2 and UV/PDS, especially UV/NH_2Cl, are limited. Moreover, UV photolysis of oxidants can generate various PRSs, including •OH, •Cl, and $•SO_4^-$; therefore, generated intermediates and the transformation pathway may vary for different UV-based AOPs. To the best of our knowledge, products comparisons of GSM and 2-MIB under various UV-based AOPs have not yet been compared. Information regarding the performance of UV/NH_2Cl for the elimination of GSM and 2-MIB and the corresponding transformation pathway is also scarce.

Therefore, this study was proposed to provide some guidance for eliminating GSM and 2-MIB in UV-based AOPs for full-scale engineering applications. The objectives of this study were: (1) to compare the degradation of GSM and 2-MIB by different UV-based AOPs, including UV/H_2O_2, UV/PDS, UV/HOCl, and UV/NH_2Cl within a photoreactor made of stainless steel with reflective inner surfaces; (2) to determine the kinetics of GSM and 2-MIB degradation and establish dynamic models for the four UV-based AOPs; (3) to identify and compare the degradation intermediates for the four UV-based AOPs, and propose a possible target compound transformation pathway.

2. Materials and methods

2.1. Chemical reagents

Chemical solutions were prepared with reagent-grade deionized (DI) water (resistivity = 18.2 mΩ cm^{-1}) applying a Milli-Q Reference system (Merck KGaA, Darmstadt, Germany). GSM and 2-MIB were obtained from Wako Pure Chemical Industries, Ltd. The GSM and 2-MIB standard solutions were supplied by Sigma–Aldrich. Sodium hypochlorite solution (NaClO, 5%), hydrogen peroxide solution (H_2O_2, 30% w/w) and methanol (HPLC grade, 99.9% purity) were obtained from Aladdin (Shanghai, China). Peroxydisulfate (PDS, 99% purity), ammonium chloride (NH_4Cl, > 99.5% purity), and anisole (AS, > 99% purity) were purchased from J&K. Benzoic acid (BA, > 99.5% purity) and *tert*-butyl alcohol (TBA, 99.5% purity) were purchased from the Alfa Assar.

2.2. Experimental setup

A 300 mL photoreactor made of stainless steel with reflective inner surfaces equipped with a 10 W low-pressure mercury lamp was used for photochemical experiments (LYL/A-UV 10 W, Guangdong Liang Yue Liang Photoelectric Technology Co., Ltd, China) (Fig. 1). And the reaction system is mixed through continuous air-purging. The wavelength of the lamp's maximum emissive power was 254 nm. The UV fluence rate (I_0) measured using potassium ferrioxalate was 4.35×10^{-6} E L^{-1} s^{-1}. The degradation of GSM and 2-MIB in UV-based AOPs was created by adding oxidant solution to the PBS and environmental water sample. The pH (7.2) of the reaction system was adjusted by adding 5 mM PBS.

The degradation of GSM and 2-MIB was conducted applying a reaction solution containing 0.1 mM oxidants (H_2O_2, PDS, HOCl, or NH_2Cl) and 110 ng L^{-1} GSM and/or 130 ng L^{-1} 2-MIB in the photoreactor. TBA (100 mM), methyl alcohol (MeOH) (100 mM) or acetate (6.3 mM) was added to the reaction system to investigate the photolysis rates of various oxidants. The reaction was initiated by UV irradiation. Environmental water samples were collected on January 5, 2021 (Tianjin, China) (SI Table S1) and filtered using 0.45 μm membranes. 1 mL of the samples were collected intervals from a narrow opening of the photoreactor and immediately mixed with sodium thiosulfate. Results are presented as the average values with at least twice tests.

2.3. Analytical methods

2.3.1. Methods for the determination of target compounds

Concentrations of GSM and 2-MIB and the transformation products (TPs) were analyzed using gas chromatography–mass spectrometry (GC-MS, Agilent 7890B-5977B, USA) coupled with solid phase microextraction and an HP-5MS column (30 m × 0.25mm × 0.25 μm, Agilent, USA). The TPs were determined according to the MS database of Agilent (NIST14.L). The carrier gas was high-purity He (99.99%, Rising Corp., China) at a flow rate of 0.8 mL min^{-1}. The injection port operated in a splitless mode with the temperature maintained at 250 °C. The oven temperature profile imitated at 40 °C for 4 min, increased to 250 °C at a rate of 10 °C·min^{-1} and then was maintained for 5 min. The MS ion source temperature, the four-stage rod temperature, the auxiliary heating zone and the solvent delay was respectively 230 °C, 150 °C, 280 °C, for 8 min. For the selected ion monitoring mode, *m/z* values of 95 and 108 for 2-MIB and *m/z* values of 112 and 125 for GSM were monitored. NB, BA, and AS were analyzed using a UV diode-array detector (DAD) coupled with SHIMADZU LC-2030C system equipped with a SHIMADZU C18 column (2.1 mm × 150 mm, 5 μm). Isocratic elution using methanol and 0.1% phosphoric acid was used as the mobile phase. The peak areas of NB, BA, and AS were quantified at 275 nm, 230 nm and 220 nm, respectively. The concentrations of H_2O_2, HOCl, NH_2Cl, and PDS were analyzed using *N,N*-diethyl-*p*-phenylenediamine method (Gokulakrishnan et al., 2016; Moore et al., 1984; Satterfield and Bonnell, 1955).

2.3.2. Methods for the determination of the second-order rate constants between GSM and 2-MIB and PRS

The second-order rate constants of GSM and 2-MIB with PRS (including •OH, •Cl, and $•SO_4^-$) were measured using the competition kinetic method, as described in detail in our previous studies (Ashton et al., 1995; Sun et al., 2019; Zhang et al., 2016) (SI Text S1). NB ($k_{NB/\cdot OH} = 4 \times 10^9\ M^{-1}\cdot s^{-1}$), BA ($k_{\cdot OH/BA} = 5.9 \times 10^9\ M^{-1}\cdot s^{-1}$, $k_{\cdot Cl/BA} = 1.8 \times 10^{10}\ M^{-1}\cdot s^{-1}$) (Buxton et al., 1988; Martire et al., 2001) and ($k_{\cdot OH/AS} = 7.8 \times 10^9\ M^{-1}\cdot s^{-1}$, $k_{SO_4^{\cdot-}/AS} = 4.9 \times 10^9\ M^{-1}\cdot s^{-1}$) (Liang and Su, 2009) were employed as the reference compounds for determining the second-order rate constants of •OH, •Cl, and $•SO_4^-$ reacting with GSM and 2-MIB.

2.3.3. Method for the determination of $[PRS]_{ss}$

Commonly, $[PRS]_{ss}$ is codetermined by the generation rate of PRS and the scavenging effect in the reaction system (Eq. (7)):

$$k_{target\ compound} = k_{1PRS,target\ compound}\cdot[PRS_1]_{ss} + k_{2PRS,target\ compound}\cdot[PRS_2]_{ss} + \ldots$$

$$k_{target\ compound} = k_{1PRS,target\ compound}\cdot[PRS_1]_{ss} + k_{2PRS,target\ compound}\cdot[PRS_2]_{ss} + \ldots \quad (6)$$

$$[PRS]_{ss} = \frac{Generation\ rate}{Scavenging\ effect} \quad (7)$$

In the reaction system, the scavenging effect (S.E.) was mainly determined by the scavenger capacity (S_c, s^{-1}) of the water matrix (H_2O/OH^-, NO_2^-, HCO_3^-, DOM etc.) and the self-scavenging effect of the oxidant.

$$\begin{aligned} S.E. &= k_{PRS/oxidant}\cdot[oxidant] + k_{PRS/H2O}\cdot[H_2O] + k_{PRS/OH-}\cdot[OH^-] \\ &\quad + k_{PRS/NO2-}\cdot[NO_2^-]\cdot + k_{PRS/HCO3-}\cdot[HCO_3^-] + k_{PRS/NOM}\cdot[NOM] + \ldots \\ &= k_{PRS/oxidant}\cdot[Oxidant] + k_{PRS/H2O}\cdot[H_2O] + k_{PRS/OH-}\cdot[OH^-] + \sum k_i\cdot[C_i] \end{aligned} \quad (8)$$

As the second-order rate constants between the PRS and oxidants and the water matrix can be easily obtained in the literatures, this study focused on the rate of PRS generation, which was determined by the direct photolysis rate of the oxidant (*-dC/dt*), which can be expressed as ($\lambda = 254$ nm in this study):

$$Generation\ Rate = -\frac{dC}{dt} = \Phi\cdot I_a = \Phi\cdot I_0\cdot F_s\cdot F_c \quad (9)$$

where I_a (Einstein·L^{-1}·s^{-1}) is the specific rate of light absorption, Φ (mol·$Einstein^{-1}$) is the quantum yield of oxidant, I_0 (Einstein·L^{-1}·s^{-1}) is the volumetric light irradiance, F_s is the fraction of light absorbed by the system, and F_c is the fraction of light absorbed by the oxidant. F_s and F_c can be further expressed as:

$$F_s = 1 - 10^{-(A_b\ +\varepsilon\cdot C)\cdot l} \quad (10)$$

$$F_{c\lambda} = \frac{\varepsilon\cdot C}{A_b + \varepsilon\cdot C} \quad (11)$$

where A_b is the absorption coefficient of the water matrices (cm^{-1}), ε is the molar absorption coefficient of the target compound ($M^{-1}\cdot cm^{-1}$), and l is the effective optical path length (cm). Eq. (9) can be further expressed as: Generation

$$Generation\ \ Rate\ = I_0\cdot\Phi\cdot\left(1 - 10^{-(A_b\ +\varepsilon\cdot C)\cdot l}\right)\cdot\left(\frac{\varepsilon\cdot C}{\varepsilon\cdot C + A_b}\right) \quad (12)$$

2.4. Dynamic modeling

A dynamic model was developed to simulate the degradation of GSM and 2-MIB in UV-based AOPs using the SimBiology application in MATLAB 2016b. The model involves a group of elementary chemical reactions. Reactions involved in UV-based AOPs and corresponding rate constants between radicals and water solutes were obtained from previous studies (SI Table S2) (Das, 2001; Kim et al., 2014; Qian et al., 2016; Sun et al., 2019; Zhang et al., 2016). The concentration of each species (including the radical concentrations, pollutant concentrations, and water solutes concentrations) is the objective function of this model. The photolysis rate of the oxidant and the rate constants between target compounds and PRS were calculated in this study. By applying the photolysis rate of the oxidant and the rate constants between target compounds and PRS, the concentration of PRS and GSM and 2-MIB can be simulated using the dynamic model. Notably, the model in this study was developed based on the hypothesis that the degradation of GSM and 2-MIB is mainly dependent on PRS (i.e., •OH, •Cl, and $•SO_4^-$).

3. Results and discussion

3.1. Degradation of GSM and 2-MIB by UV-based AOPs in PBS and environmental water samples

The degradation of 0.603 nM (110 ng L^{-1}) GSM and 0.773 nM (130

Fig. 1. Illustrations of photolysis experimental setup.

ng L^{-1}) 2-MIB under different UV-based AOPs in PBS and environmental water samples was conducted in a photoreactor with reflective inner surfaces (Fig. 2). Both GSM and 2-MIB were stable in the presence of 0.1 mM oxidant in the dark, indicating the oxidant alone cannot transform these odor compounds. The degradation of GSM and 2-MIB under UV irradiation alone within 180 s can also be neglected, which was consistant with their weak light absorption at 254 nm (Kutschera et al., 2009). In contrast, rapid degradation of GSM and 2-MIB occurred in the four UV-based AOPs, suggesting that GSM and 2-MIB were predominantly degenerated by reactive species generated by photolysis of oxidants in the two water matrices (SI Fig. S1). The degradation of GSM in UV-based AOPs was similar to that observed for 2-MIB, which followed pseudo-first-order kinetics in the two water matrices (SI Fig. S1).

In PBS, the pseudo-first-order rate constants for GSM degradation by UV/H_2O_2, UV/PDS, UV/HOCl and UV/NH_2Cl were calculated to be 2.81×10^{-2} s^{-1}, 2.63×10^{-2} s^{-1}, 6.09×10^{-3} s^{-1} and 9.43×10^{-3} s^{-1}, respectively. The pseudo-first-order rate constants for 2-MIB were 2.50×10^{-2} s^{-1}, 2.80×10^{-2} s^{-1}, 4.99×10^{-3} s^{-1} and 7.41×10^{-3} s^{-1}, respectively. The degradation rates of both GSM and 2-MIB in the PBS ranked were: UV/PDS ≈ UV/H_2O_2 > UV/NH_2Cl > UV/HOCl in PBS. In environmental water sample, the degradation rates of GSM by UV/H_2O_2, UV/PDS, UV/HOCl and UV/NH_2Cl were calculated to be 3.43×10^{-3} s^{-1}, 1.16×10^{-3} s^{-1}, 1.04×10^{-3} s^{-1} and 6.48×10^{-4} s^{-1}, respectively. Additionally, the degradation rates for 2-MIB were 3.53×10^{-3} s^{-1}, 1.20×10^{-3} s^{-1}, 8.63×10^{-4} s^{-1} and 4.88×10^{-4} s^{-1}, respectively. Compared with the degradation rate in PBS, those of GSM and 2-MIB significantly decreased in the environmental water sample, with the declines being about 82.7%–95.7%.

As discussed above, the degradation of GSM and 2-MIB in the four UV-based AOPs was predominantly dependent on the PRS produced via photolysis of oxidants. Therefore, the degradation rates of GSM and 2-MIB were determined by the second-order rate constants of the reaction between PRS and the target compounds ($k_{PRS,target\ compound}$) and the steady-state concentration of PRS ($[PRS]_{ss}$) (Eq. (6)). For a certain UV-based AOP, the $k_{PRS,target\ compound}$ was constant, and the degradation rates of GSM and 2-MIB were determined by the $[PRS]_{ss}$. Commonly, $[PRS]_{ss}$ is codetermined by the generation rate of PRS and the scavenging effect in the reaction system (Eq. (7)).

In this study, the A_b of the environmental water sample was 0.039 cm^{-1} ($A_b = 0$ in PBS) at 254 nm, which was comparable (0.0382 cm^{-1} for NH_2Cl) or much greater (0.0062 cm^{-1} for HOCl, 0.0022 cm^{-1} for PDS, and 0.0018 cm^{-1} for H_2O_2) than that of the 0.1 mM oxidant (Miklos et al., 2018; Sun et al., 2019). Therefore, the generation rate of PRS, which was mostly dependent on the light absorption fraction of the oxidant in the reaction system, significantly decreased in the environmental water sample. Specifically, applying Eq. (12), the generation rates of PRS were theoretically decreased by 95.6%, 94.7%, 86.3% and 50.5% for UV/H_2O_2, UV/PDS, UV/HOCl and UV/NH_2Cl, respectively. It is worth-noting that this light-shielding effect from environmental water matrix has been commonly neglected in studies within thin-optical pathlength photoreactors. In addition to light-shielding effect to decrease PRS production rates, the existence of radical scavengers in the environmental water matrix (such as NO_2^-, HCO_3^-, and dissolved organic matter (DOM)) can also compete with the target compounds to consume the PRS, thus increased the scavenging effect. Therefore, the observed GSM and 2-MIB degradation rates in the environmental water sample, which were significantly less than those observed in the PBS, are reasonably expected.

To better evaluate the PRS in the kinetics study and characterize the transformation pathway of GSM and 2-MIB in the four UV-based AOPs, the following research was conducted in a PBS.

3.2. Kinetics study of GSM and 2-MIB in the four UV-based AOPs

3.2.1. Reaction rate constants of primary reactive species with GSM and 2-MIB

To establish the dynamic model of the photoreactor with reflective inner surfaces, the $k_{PRS,target\ compound}$ were investigated in a PBS. Although UV photolysis of oxidants can yield PRS, certain yielded PRS may subsequently react with the water matrix and transform into other reactive species. The contribution of the weak reactivity and high selectively of •NH_2 and secondary radicals (e.g., •Cl_2^-, •CO_3^-, and •ClO) (Lei et al., 2019; Neta et al., 1978; Poskrebyshev et al., 2003; Sun et al., 2016, 2019) was not considered in this study. In engineering applications, PRS (i.e., •OH, •Cl, and •SO_4^-) were considered as the major contributors to the four UV-based AOPs.

The second-order rate constants of the reactions between PRS and GSM and 2-MIB in the UV-based AOPs were investigated by applying the competition kinetics method (Table 1). NB ($k_{•OH/NB} = 4.0 \times 10^9$ M^{-1} s^{-1}), BA ($k_{•OH/BA} = 5.9 \times 10^9$ $M^{-1}{\cdot}s^{-1}$, $k_{•Cl/BA} = 1.8 \times 10^{10}$ $M^{-1}{\cdot}s^{-1}$), and AS ($k_{•OH/AS} = 7.8 \times 10^9$ $M^{-1}{\cdot}s^{-1}$, $k_{SO_4^{•-}} = 4.9 \times 10^9$ $M^{-1}{\cdot}s^{-1}$) were used as reference compounds (Ashton et al., 1995; Buxton et al., 1988; Liang and Su, 2009; Martire et al., 2001). The second-order rate constants of the GSM and 2-MIB with •OH, •Cl and •SO_4^- can generally be ranked as $k_{•OH/Compound}$ ($k_{•OH/GSM} = 1.10 \times 10^{10}$ M^{-1} s^{-1}, $k_{•OH/2\text{-}MIB} = 8.46 \times 10^9$ M^{-1} s^{-1}) > $k_{•Cl//Compound}$ ($k_{•Cl/GSM} = 2.74 \times 10^9$ M^{-1} s^{-1}, $k_{•Cl/2\text{-}MIB}$ =

Table 1
The second order rate constants of reactions between GSM and 2-MIB and PRS.

Contaminant	•OH ($M^{-1}s^{-1}$)	•Cl ($M^{-1}s^{-1}$)	$SO_4^{•-}$ ($M^{-1}s^{-1}$)
GSM	1.1×10^{10} [a]	2.74×10^9 [a]	9.99×10^8 [a]
	$0.57–1.4 \times 10^{10}$ [b]	n.a	7.60×10^8 [b]
2-MIB	8.46×10^9 [a]	2.57×10^9 [a]	4.60×10^8 [a]
	$4.3–8.2 \times 10^9$ [b]	n.a	4.20×10^8 [b]

n.a means data were not available in previous studies
[a] Measured in this study.
[b] References (Peter and Von Gunten, 2007; Xie et al., 2015).

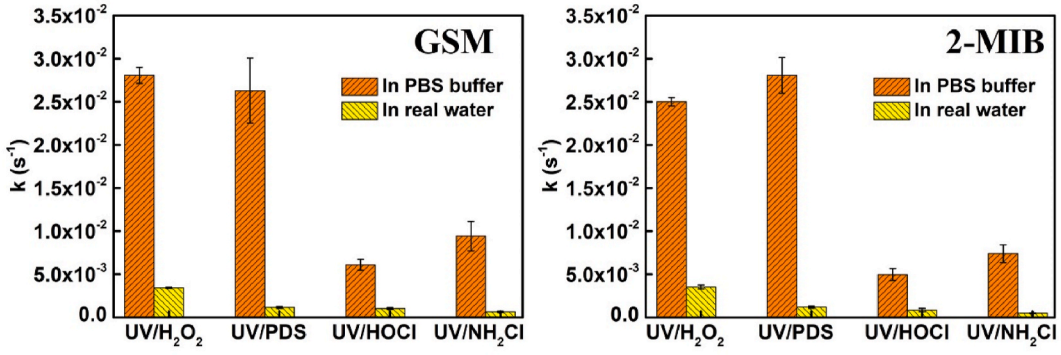

Fig. 2. Degradation rates of GSM and 2-MIB in UV-based AOPs in PBS and environmental water sample. Initial radical oxidants concentration were 0.10 mM. Reaction employed 0.603 nM (110 ng L^{-1}) and 0.773 nM (130 ng L^{-1}) initial concentration of GSM and 2-MIB, respectively.

$2.57 \times 10^9\ M^{-1}\ s^{-1}) > k_{\bullet SO4\text{-}/Compound}$ ($k_{\bullet SO4\text{-}/GSM} = 9.99 \times 10^8\ M^{-1}\ s^{-1}$, $k_{\bullet SO4\text{-}/2\text{-}MIB} = 4.60 \times 10^8\ M^{-1}\ s^{-1}$). The rate constants between $\bullet OH/\bullet SO_4^-$ and GSM/2-MIB determined in this study are comparable to the data reported in previous studies (Table 1) (Peter and Von Gunten, 2007; Xie et al., 2015).

3.2.2. Determination of [PRS]ss for photoreactors with reflective inner surfaces

$[PRS]_{ss}$ is codetermined by the generation rate of PRS and the scavenging effect in the reaction system (Eq. (7)). As the second-order rate constants between the PRS and oxidants and the water matrix can be easily obtained in the literatures, this study focused on the rate of PRS generation. In engineering applications, photoreactors are designed to utilize as much UV light as possible (such as using reflective surfaces). Consequently, they are designed to maximize the light remaining within the photoreactor and being subsequently absorbed by the water matrices (Fig. 1). Generally, the actual path length in an engineering system is sufficiently long in photoreactor with reflective surfaces. Because the path length (l) is the exponent term in Eq. (10), F_s approaches one, Eq. (12) can be further expressed as:

$$Generation\ \ Rate\ = I_0 \cdot \Phi \cdot \left(\frac{\varepsilon \cdot C}{\varepsilon \cdot C + A_b}\right) \quad (13)$$

For a specific photoreactor (fixed with UV light and size), I_0 was determined by UV lamp and was consistent under ideal conditions in PBS ($A_b = 0$). The observed UV fluence rate of an actual photoreactor at the bench-scale was lesser than would be expected under ideal conditions. This was primarily caused by the reactor walls absorbing light, which resulted in attenuated UV light energy. The light irradiance of the photoreactor (a constant value with a fixed UV light) contains two parts: the light absorption of the reaction system (oxidant and the background water matrix [$A_b = 0$ for PBS], $I_{absorbed}$) and the energy losses upon reflection off the reactor wall (I_{loss}). Energy losses were correlated with the number of reflections, and $I_{absorbed}$ decreased with an increasing number of reflections (i.e., increasing light path for a certain photoreactor). In general, lower oxidant light absorption led to a longer effective light path, and consequently, a lower $I_{absorbed}$. Notably, the photolysis rate of the oxidant varied with the type and concentration of oxidants in the photoreactor containing reflective inner surfaces. This differed from the observations when the quartz reactor (with a constant path length) were utilized. Therefore, the $[PRS]_{ss}$ should be simulated based on the photolysis rate of the oxidant at certain concentrations (0.1 mM in this study). Notably, $I_{absorbed}$ was related to the effective light path of the photoreactor.

For the measurement of the photolysis rate of the oxidant, as the UV photolysis of oxidant could yield radicals, the observed overall decay of oxidant in UV irradiation incorporated both direct photolysis and subsequent scavenging by radicals (Chuang et al., 2017). To determine the direct photolysis rate of oxidant, TBA and MeOH were applied as radical scavengers because TBA and MeOH could rapidly react with $\bullet OH/\bullet Cl$ and $\bullet SO_4^-$ ($k_{\bullet OH/TBA} = 6.0 \times 10^8\ M^{-1}\cdot s^{-1}$ $k_{\bullet Cl/TBA} = 1.5 \times 10^9\ M^{-1}\cdot s^{-1}$, $k_{\bullet SO4\text{-}/MeOH} = 1.0 \times 10^7\ M^{-1}\cdot s^{-1}$) (NIST) and have no absorption at 254 nm. Moreover, previous studies have demonstrated that using alcohol as a radical quencher may promote oxidant chain decomposition during photolysis (Chuang et al., 2017). Consequently, the photolysis rates of oxidants with acetate (6.3 mM) and TBA/MeOH (100 mM) were compared in this study. As shown in Fig. 3, the decomposition of the oxidant under UV irradiation followed first-order kinetics under all conditions, and the degradation rates of the oxidants with TBA/MeOH and acetate at pH 7.2 were negligibly different (SI Fig. S2). In addition, the self-decomposition of oxidants in the dark can be neglected within the 8 min (SI Fig. S2). By applying the photolysis rate under conditions including TBA/MeOH, the $[PRS]_{ss}$ of UV-based AOPs with certain oxidant concentrations can be simulated.

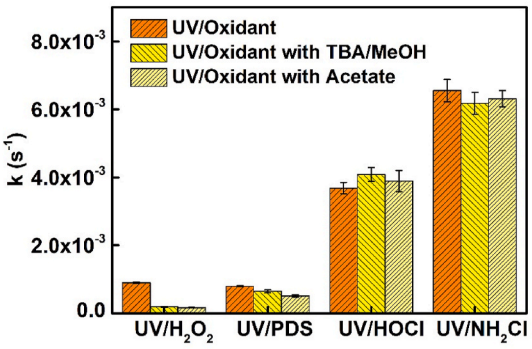

Fig. 3. Photolysis rate of oxidants under UV irradiation at pH 7.2. Reactions employed 0.10 mM initial concentration of oxidants in 5 mM PBS, initial TBA/MeOH and acetate concentrations were 100 mM and 6.3 mM, respectively.

3.2.3. Dynamic model for UV-based AOPs for photoreactors with reflective inner surfaces

By applying the degradation rate of oxidants with TBA/MeOH and $k_{PRS,target\ compound}$, a dynamic model to simulate the degradation of GSM and 2-MIB in a photoreactor with reflective inner surfaces in the four UV-based AOPs was established by SimBiology. Notably, the model was developed based on the hypothesis that the degradation of GSM and 2-MIB in UV-based AOPs was mainly depends on the PRSs, including $\bullet OH$, $\bullet Cl$, and $\bullet SO_4^-$. As shown in Fig. 4, the degradation of GSM and 2-MIB was roughly consistent with the experimental data for the four UV-based AOPs. This indicated that the contribution of other radicals (i.e., $\bullet NH_2$, $\bullet Cl_2^-$, $\bullet ClO$, and $\bullet CO_3^-$), except for the $\bullet OH$, $\bullet Cl$, and $\bullet SO_4^-$ may be neglected in this study. Moreover, the successful simulation of GSM and 2-MIB degradation further supported the accuracy of $k_{PRS,target\ compound}$ in this study. The model established based on the photoreactor with an inner reflective surface is promising for engineering applications of UV-based AOPs.

3.3. Transformation products of GSM in UV-based AOPs

Based on the above results, direct photolysis and the oxidant-alone reaction of GSM and 2-MIB within 8 min in this study may be negligible. GSM and 2-MIB were mainly degraded by $\bullet OH$, $\bullet Cl$, and $\bullet SO_4^-$, and intermediates generated under UV-based AOPs in the PBS were identified, including UV/H_2O_2, UV/PDS, UV/HOCl, and UV/NH_2Cl. As GSM and 2-MIB demonstrated the same degradation kinetics and followed the same pathways as those of the formation of degradation products (Ma et al., 2018), GSM was selected as the model compound for subsequent research.

In this study, 8, 7, 8, and 11 degradation intermediates were observed for UV/H_2O_2, UV/PDS, UV/HOCl, and UV/NH_2Cl, respectively (Fig. 5). Among these, *trans*-1,10-dimethyl-trans-9-decalinol (P1), 1,3-dimethyladmantane (P2),4-dimethyladmantane (P3) and *cis*-1-ethyl-ideneoctahydro-7a-methyl-1H-indene (P4) were identified in all four UV-based AOPs, which was similar to those from the previous studies conducted in UV/HOCl (Kim et al., 2016; Ma et al., 2018). However, subsequent ring-opening intermediates were different in the four UV-based AOPs. For UV/H_2O_2 and UV/PDS, ring-opening reactions attributed to radical attack on GSM and P1–P4 contribute to the generation of intermediates P5–P8 and P5, P9 and P10 for UV/H_2O_2 and UV/PDS, respectively. As for UV/HOCl and UV/NH_2Cl, in addition to full ring opening products, five and six-membered rings were also created because of the ring opening and OH-addition reaction (SI Table S3). Although the ring-opening products were not identical to those reported in previous studies (Kim et al., 2016; Ma et al., 2018), transformation products were similar, including ketones, aldehydes, alcohols, cycloalkanes, and olefins in UV/HOCl.

Based on the transformation products detected above, we proposed

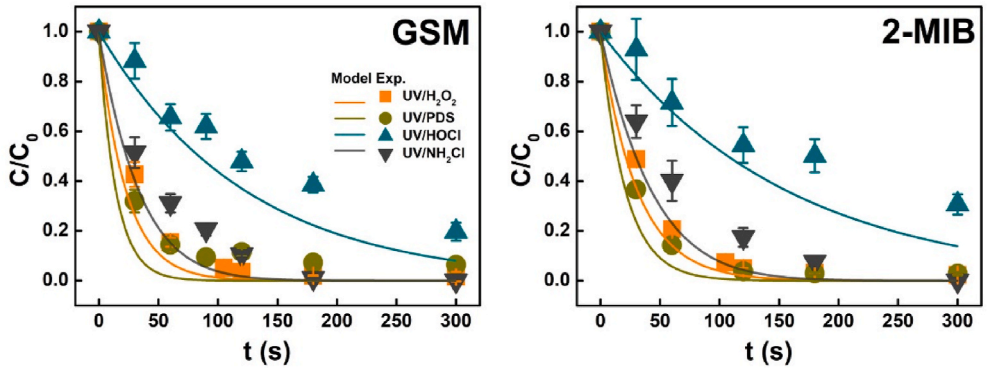

Fig. 4. Degradation of GSM and 2-MIB in UV-based AOPs in PBS at pH 7.2. Initial oxidants concentration were 0.10 mM. Reaction employed 0.603 nM (110 ng L^{-1}) and 0.773 nM (130 ng L^{-1}) initial concentration of GSM and 2-MIB, respectively.

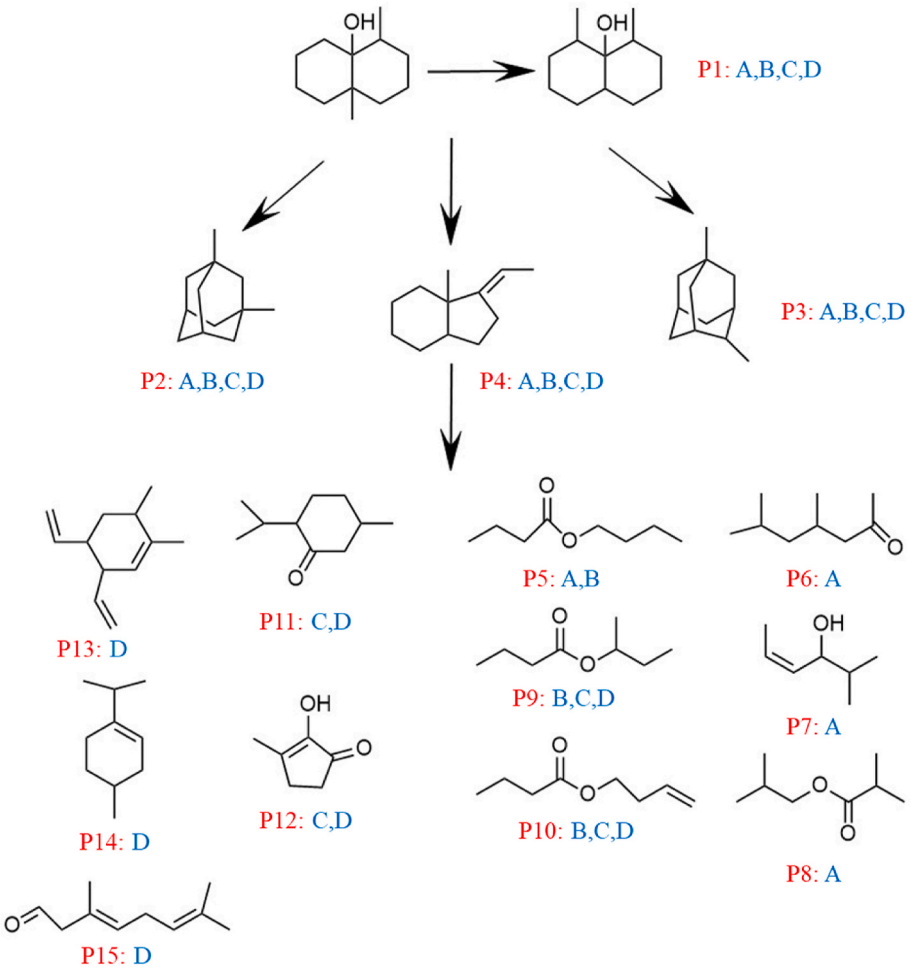

Fig. 5. Proposed transformation products of GSM under four UV-based AOPs in 5 mM PBS buffer at pH 7.2. A: UV/H_2O_2 (P1–P8); B: UV/PDS (P1–P5, P9–P10); C: UV/HOCl (P1–P4, P9–P12); D: UV/NH_2Cl (P1–P4, P9–P15).

possible degradation pathways of GSM in the four UV-based AOPs. The transformation of GSM mainly involves dehydration, rearrangement, and ring opening, among which dehydration plays a key role in UV-based AOPs. Two directly dehydrated intermediates P2 and P3, were identified, which could then be transformed to P4 by hydration and rearrangement. P1 was possible generated by the dehydration and followed by OH-addition and π-bond rearrangement during the degradation of GSM. GSM and P1–P4 were then transformed into five-member and six-member rings or full ring opening products by ring opening and OH-addition reactions.

Similar to the degradation pathway of GSM, the elimination of H_2O molecules also play a dominant role during the deterioration of 2-MIB in UV-based AOPs, followed by ring opening due to radical attack and subsequent structural rearrangement (Ma et al., 2018). Detailed results are not discussed in this study.

4. Conclusions

This study investigated degradation kinetics and transformation pathways of GSM and 2-MIB in four UV-based AOPs in a photoreactor with reflective inner surfaces. The GSM and 2-MIB could be effectively removed under UV-based AOPs in PBS. The light absorption and the existence of radical scavengers in the environmental water sample had a negative effect on the degradation efficiencies of GSM and 2-MIB. A dynamic model to simulate the degradation of GSM and 2-MIB in a photoreactor with reflective inner surfaces in the four UV-based AOPs was established by applying the direct photolysis rate of oxidants and $k_{PRS,target\ compound}$. Furthermore, the transformation products of GSM in the four UV-based AOPs were determined and possible transformation pathways were proposed. The main transformation ways for GSM and 2-MIB included dehydration, rearrangement, and ring opening. The results of our study based on a photoreactor with inner reflective surfaces are promising for engineering applications of UV-based AOPs.

Author statement

Xiao Su and Peizhe Sun designed the experiments and interpretated the data. Tan Meng and Xiao Su carried out all the experiments and measurements. Tan Meng and Peizhe Sun wrote the paper.

Declaration of competing interest

The authors declare that they have no known competing financial interests or personal relationships that could have appeared to influence the work reported in this paper.

Acknowledgement

This work was supported by the project from National Natural Science Foundation of China (No. 22176141), the Beijing Outstanding Young Scientist Program (BJJWZYJH01201910004016) and China Postdoctoral Science Foundation (No. 2020M670671).

Appendix A. Supplementary data

Supplementary data to this article can be found online at https://doi.org/10.1016/j.chemosphere.2022.135611.

References

Ashton, L., Buxton, G.V., Stuart, C.R., 1995. Temperature dependence of the rate of reaction of OH with some aromatic compounds in aqueous solution. Evidence for the formation of a π-complex intermediate? J. Chem. Soc. Faraday. Trans. 91 (11), 1631–1633.

Agus, E., Lim, M.H., Zhang, L., Sedlak, D.L., 2011. Odorous compounds in municipal wastewater effluent and potable water reuse systems. Environ. Sci. Technol. 45 (21), 9347–9355.

Buxton, G.V., Greenstock, C.L., Helman, W.P., Ross, A.B., 1988. Critical review of rate constants for reactions of hydrated electrons, hydrogen atoms and hydroxyl radicals (•OH/•O−) in aqueous solution. J. Phys. Chem. Ref. Data 17 (2), 513–886.

Chuang, Y.H., Chen, S., Chinn, C., Mitch, W.A., 2017. Comparing the UV/monochloramine and UV/free chlorine advanced oxidation processes (AOPs) to the UV/hydrogen peroxide AOP under scenarios relevant to potable reuse. Environ. Sci. Technol. 51 (23), 13859–13868.

Das, T.N., 2001. Reactivity and role of SO_5 center dot- radical in aqueous medium chain oxidation of sulfite to sulfate and atmospheric sulfuric acid generation. J. Phys. Chem. A 105 (40), 9142–9155.

Fang, J., Fu, Y., Shang, C., 2014. The roles of reactive species in micropollutant degradation in the UV/free chlorine system. Environ. Sci. Technol. 48 (3), 1859–1868.

Gokulakrishnan, S., Mohammed, A., Prakash, H., 2016. Determination of persulphates using N,N-diethyl-p-phenylenediamine as colorimetric reagent: oxidative coloration and degradation of the reagent without bactericidal effect in water. Chem. Eng. J. 286, 223–231.

Jo, C.H., Dietrich, A.M., Tanko, J.M., 2011. Simultaneous degradation of disinfection byproducts and earthy-musty odorants by the UV/H_2O_2 advanced oxidation process. Water Res. 45 (8), 2507–2516.

Kim, D.H., Lee, J., Ryu, J., Kim, K., Choi, W., 2014. Arsenite oxidation initiated by the UV photolysis of nitrite and nitrate. Environ. Sci. Technol. 48 (7), 4030–4037.

Kim, T.-K., Moon, B.-R., Kim, T., Kim, M.-K., Zoh, K.-D., 2016. Degradation mechanisms of geosmin and 2-MIB during UV photolysis and UV/chlorine reactions. Chemosphere 162, 157–164.

Kutschera, K., Bornick, H., Worch, E., 2009. Photoinitiated oxidation of geosmin and 2-methylisoborneol by irradiation with 254 nm and 185 nm UV light. Water Res. 43 (8), 2224–2232.

Lei, Y., Cheng, S., Luo, N., Yang, X., An, T., 2019. Rate constants and mechanisms of the reactions of Cl(*) and Cl_2(*-) with trace organic contaminants. Environ. Sci. Technol. 53 (19), 11170–11182.

Liang, C.J., Su, H.W., 2009. Identification of sulfate and hydroxyl radicals in thermally activated persulfate. Ind. Eng. Chem. Res. 48 (11), 5558–5562.

Ma, L., Wang, C., Li, H., Peng, F., Yang, Z., 2018. Degradation of geosmin and 2-methylisoborneol in water with UV/chlorine: influencing factors, reactive species, and possible pathways. Chemosphere 211, 1166–1175.

Martire, D.O., Rosso, J.A., Bertolotti, S., Le Roux, G.C., Braun, A.M., Gonzalez, M.C., 2001. Kinetic study of the reactions of chlorine atoms and Cl(2)(center dot-)radical anions in aqueous solutions. II. Toluene, benzoic acid, and chlorobenzene. J. Phys. Chem. A 105 (22), 5385–5392.

Miklos, D.B., Remy, C., Jekel, M., Linden, K.G., Drewes, J.E., Hubner, U., 2018. Evaluation of advanced oxidation processes for water and wastewater treatment - a critical review. Water Res. 139, 118–131.

Moore, H.E., Garmendia, M.J., Cooper, W.J., 1984. Kinetics of monochloramine oxidation of N,N-diethyl-p-phenylenediamine. Environ. Sci. Technol. 18 (5), 348–353.

Neta, P., Maruthamuthu, P., Carton, P.M., Fessenden, R.W., 1978. Formation and reactivity of the amino radical. J. Phys. Chem. 82 (17), 1875–1878.

NIST. NDRL/NIST Solution Kinetics Database on the Web. http://kinetics.nist.gov/solution/.

Omur-Ozbek, P., Dietrich, A.M., 2008. Developing hexanal as an odor reference standard for sensory analysis of drinking water. Water Res. 42 (10–11), 2598–2604.

Peter, A., Von Gunten, U., 2007. Oxidation kinetics of selected taste and odor compounds during ozonation of drinking water. Environ. Sci. Technol. 41 (2), 626–631.

Poskrebyshev, G.A., Huie, R.E., Neta, P., 2003. Radiolytic reactions of monochloramine in aqueous solutions. J. Phys. Chem. A 107 (38), 7423–7428.

Qian, Y.J., Guo, X., Zhang, Y.L., Peng, Y., Sun, P.Z., Huang, C.H., Niu, J.F., Zhou, X.F., Crittenden, J.C., 2016. Perfluorooctanoic acid degradation using UV-persulfate process: modeling of the degradation and chlorate formation. Environ. Sci. Technol. 50 (2), 772–781.

Satterfield, C.N., Bonnell, A.H., 1955. Interferences in the titanium sulfate method for hydrogen peroxide. Anal. Chem. 27 (7), 1174–1175.

Srinivasan, R., Sorial, G.A., 2011. Treatment of taste and odor causing compounds 2-methyl isoborneol and geosmin in drinking water: a critical review. J. Environ. Sci. 23 (1), 1–13.

Sun, P., Lee, W.N., Zhang, R., Huang, C.H., 2016. Degradation of DEET and caffeine under UV/chlorine and simulated sunlight/chlorine conditions. Environ. Sci. Technol. 50 (24), 13265–13273.

Sun, P., Meng, T., Wang, Z., Zhang, R., Yao, H., Yang, Y., Zhao, L., 2019. Degradation of organic micropollutants in UV/NH_2Cl advanced oxidation process. Environ. Sci. Technol. 53 (15), 9024–9033.

Wang, C., Yu, J., Guo, Q., Sun, D., Su, M., An, W., Zhang, Y., Yang, M., 2019. Occurrence of swampy/septic odor and possible odorants in source and finished drinking water of major cities across China. Environ. Pollut. 249, 305–310.

Wang, D., Bolton, J.R., Andrews, S.A., Hofmann, R., 2015. UV/chlorine control of drinking water taste and odour at pilot and full-scale. Chemosphere 136, 239–244.

Wang, L., Zhang, Q., Chen, B., Bu, Y., Chen, Y., Ma, J., Rosario-Ortiz, F.L., Zhu, R., 2020. Some issues limiting photo(cata)lysis application in water pollutant control: a critical review from chemistry perspectives. Water Res. 174, 115605.

Xie, P., Ma, J., Liu, W., Zou, J., Yue, S., Li, X., Wiesner, M.R., Fang, J., 2015. Removal of 2-MIB and geosmin using UV/persulfate: contributions of hydroxyl and sulfate radicals. Water Res. 69, 223–233.

Zhang, R., Yang, Y., Huang, C.H., Zhao, L., Sun, P., 2016. Kinetics and modeling of sulfonamide antibiotic degradation in wastewater and human urine by UV/H_2O_2 and UV/PDS. Water Res. 103, 283–292.